

Multimode VCSEL Thermal and Spatial Model

Abstract. We present a VCSEL model that addresses the spatial dependence and thermal behavior of VCSELs based on multimode rate equations without sacrificing the numerical efficiency demanded by the circuit-level simulation of optoelectronic systems. The model is more comprehensive and parameters are easier to determine. The equivalent circuit of the model and expressions of circuit elements are given. It is implemented into SPICE-like simulators to simulate the dc, ac and transient features of VCSELs. The simulated results exhibit good agreements with references.

Streszczenie. Zaprezentowano model lasera typu VCSEL (vertical cavity surface emitting laser). Analizowano właściwości przestrzenne i termiczne. Zaproponowano schemat zastępczy modelu i przeprowadzono symulacje. (Termiczny i przestrzenny model lasera typu VCSEL)

Keywords: Vertical-Cavity Surface-Emitting Laser (VCSEL), Rate-equation, Thermal model, Spatial model.

Słowa kluczowe: laser VCSEL, modelowanie.

Introduction

In recent years, the characteristics of VCSELs have improved enormously [1-2] that they have attracted more considerable interest due to their advantages, and they have been studied as elements of a variety of systems, including multichannel optical links, smart pixel systems, optoelectronic switches, WDM applications, optical storage, and laser printing [3-4].

There are various VCSEL models presented in literatures. Some approaches employed quantum-well gain calculations and finite-element analysis to model the thermal gain, leakage, and spatial-dependence of VCSEL [5]. While these models are comprehensive, their computationally intensive nature makes them unsuitable for circuit- and system-level design and simulation. Some simpler approaches, however, have resulted in models which generally provide an incomplete picture of a VCSEL's behavior. For example, Mena [6], LIU [7] and Liang [8] presented a VCSEL model which accounts for thermal behavior, respectively. However, the models are limited to a single mode and neglect spatial effects. Morikuni [9] presented a VCSEL model which accounts for spatial effects, but neglect thermal effects and multimode behavior. The model developed by Mena [10], which accounts for thermal, spatial and multimode behavior, is comprehensive and suitable for circuit-level simulation. However, the model utilized an empirical function to describe the VCSEL's electrical characteristics. It is somewhat unpractical for the parameters of the model cannot extract directly. Moreover, the effects of temperature dependent parasitic resistance and reverse saturation current are not included in the model.

In this paper, we present a VCSEL model including thermal and spatial effects based on multimode rate-equations. A general diode, including the thermal effect of parasitic resistor and reverse saturation current, instead of an empirical function, is adopted to model the current-voltage relationship. The equivalent circuit of the model and expressions of circuit elements are given. It is really simple, and it can model basic laser behavior under both dc and non-dc conditions.

Modeling

A. Rate-equations

Many characteristics of VCSEL behavior can be modeled by a set of coupled rate equations, which describe the relation between the carrier density and photo density. The rate-equations of VCSEL including thermal and spatial effects can be expressed as

$$\begin{aligned} \frac{\partial N(r,t)}{\partial t} &= \eta_i I(r,t,T)/q - N(r,t)/\tau_n - \sum_k G_k(r,t,T) S_k(t) \psi_k(r) \\ &\quad + L_{eff}^2 \nabla^2 N(r,t)/\tau_n - I_l(N,T)/q \\ \frac{\partial S_k(t)}{\partial t} &= -S_k(t)/\tau_{pk} + \beta_k N(r,t)/\tau_n + G_k(r,t,T) S_k(t) \psi_k(r) \\ T &= T_0 + R_{th}(VI_{tot} - P_O) - \tau_{th} dT/dt \end{aligned}$$

where S_k and ψ_k are the total photon number and normalized transverse mode profile in the k th transverse mode, respectively; N is the electron populations; r denotes position; t denotes time; T denotes temperature; η_i is the current injection efficiency; I is the spatially dependent injection current; I_l is the thermal leakage current; q is the electronic charge; L_{eff} is the effective carrier diffusion length; τ_n is the electron lifetimes; G_k is the gain coefficient of k th mode; and β_k and τ_{pk} are the spontaneous-emission coupling coefficient and photon lifetime, respectively, for the k th mode; V and I_{tot} are input voltage and input current, respectively; P_O is the optical output power; T_0 is the environment temperature; R_{th} is the VCSEL's thermal impedance; τ_{th} is a thermal time constant.

B. Thermal effects modeling

The strong thermal dependence of VCSEL can account for several mechanisms. The temperature dependent parasitic resistance, reverse saturation current, optical gain and the carrier leakage of the active region all play important roles in the thermal behavior.

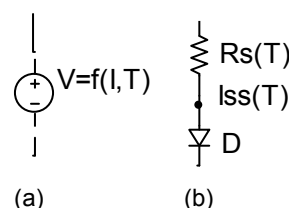


Fig.1 Model of VCSEL's electrical characteristics (a) in reference (b) in the paper

While the VCSEL's electrical characteristics could be modelled in great detail based on the complex VCSEL device structure, many references modelled them as a voltage source controlled by injected current and temperature by empirical function (shown in Fig.1(a)). The empirical function has neither unified form nor physical meaning, and its parameters are difficult to determine. Moreover, the effects of the temperature dependent parasitic resistance and reverse saturation current are not included in the model. Here we model the VCSEL as a laser diode including the effect of the temperature dependent

parasitic resistance and reverse saturation current (shown in Fig.1(b)), while the extrinsic parameters and intrinsic parameters are extracted directly by method of Gao [11]. So our thermal model is more practical than which proposed in the reference 10.

The voltage-current (V-I) characteristic of VCSEL can be described by the voltage-current (V-I) characteristic of diode as

$$V = V_T \ln[I/I_{ss}(T) + 1] + IR_s(T),$$

where V_T is thermal voltage; I_{ss} is reverse saturation current; R_s is parasitic resistance.

While the inject current increased, the temperature of VCSEL will increase, thus the parasitic resistor R_s will decrease, and saturation current I_{ss} will increase. The parasitic resistor R_s and saturation current I_{ss} are controlled by temperature. To model this thermal effect, the parasitic resistor R_s and saturation current I_{ss} are described as

$$R_s(T) = e_1/(T - e_2), \quad I_{ss}(T) = f_1 I_{ss0}(T - f_2),$$

where e_1, e_2, f_1, f_2 are fitting constants obtained from experimental data. I_{ss0} is the reverse saturation current at zero degree.

The temperature dependent gain can be expressed as a linear function of the carrier number N and incorporate the gain saturation with gain compression factor.

$$G_k(r, t, T) = G_T \left[\frac{N(r, t) - N_T}{1 + \varepsilon_{mk} S_m} \right]$$

$$G_T = G_0 \left(\frac{a_0 + a_1 T + a_2 T^2}{b_0 + b_1 T + b_2 T^2} \right)$$

$$N_T = N_{T0} \left(c_0 + c_1 T + c_2 T^2 \right)$$

where G_0 is the temperature-independent gain coefficient, N_{T0} is the temperature-independent transparency carrier number, respectively; ε_{mk} is the gain saturation term of mode k due to mode m ; $a_0, a_1, a_2, b_0, b_1, b_2, c_0, c_1, c_2$ are constants.

The leakage current can be modeled as a function of temperature and carrier number

$$I_l = I_{l0} \exp\left[\frac{-d_0 + d_1 N + d_2 N T - d_3/N}{T} \right],$$

where d_0, d_1, d_2, d_3 are constants.

C. Spatial effects modeling

Spatial effects related to the transverse variation of the active-layer carrier and mode profiles play an important role in a VCSEL's behavior as well as thermal effects. They can limit a VCSEL's performance in the turn-off transient by contributing to the secondary pulsations and so on.

The electron distribution can be representation as Bessel series expansion by

$$N(r, t) = N_0(t) - \sum_{i=1}^{\infty} N_i(t) J_0(\sigma_i r/R)$$

The photon distribution can be represented in general term by

$$\psi_k(r) = \begin{cases} \alpha_k J_k^2(u_k r/W_m), & 0 < r < W_m \\ \alpha_k K_k^2(u_k r/W_m) \cdot [J_k^2(u_k)/K_k^2(\omega_k)], & r > W_m \end{cases}$$

where α_k is the normalization constant, J_k and K_k are the Bessel functions of the first and second kind, respectively, and W_m is a characteristic mode width. u_k and ω_k are eigenvalue solution of the optical waveguide.

Then a separate electron rate equation is generated for each term in the Bessel expansion.

$$dN_0(t)/dt = [\eta_i I_0(r, t, T)/q - N_0(t)/\tau_n - I_l(N_0, T)/q] - G_T(T)$$

$$\cdot \sum_k \left[\gamma_{k0} N_0(t) - \sum_{i=1}^{\infty} \gamma_{ki} N_i(t) - \gamma_{k0} N_T(T) \right] S_k(t) / \left(1 + \sum_m \varepsilon_{mk} S_m(t) \right)$$

$$dN_j(t)/dt = \left[-\eta_j \zeta_j I_0(r, t, T)/q - (1 + h_j) N_j(t)/\tau_n \right] + G_T(T)$$

$$\cdot \sum_k \left[\phi_{jk0} N_0(t) - \sum_{i=1}^{\infty} \phi_{jki} N_i(t) - \phi_{jk0} N_T(T) \right] S_k(t) / \left(1 + \sum_m \varepsilon_{mk} S_m(t) \right)$$

$$dS_k/dt = -S_k/\tau_{pk} + \beta_k \left[I_0 N_0(t) - \sum_{i=1}^{\infty} I_i N_i(t) \right] / \tau_n + G_T(T)$$

$$\cdot \sum_k \left[\lambda_{k0} N_0(t) - \sum_{i=1}^{\infty} \lambda_{ki} N_i(t) - \lambda_{k0} N_T(T) \right] S_k(t) / \left(1 + \sum_m \varepsilon_{mk} S_m(t) \right)$$

where ζ_j is the current distribution constant; h_j is the spontaneous emission constant; and h_j is the diffusive effects coefficients described as

$$h_j = (\sigma_j L_{eff}/W)^2$$

The coefficient γ_{ki} , ϕ_{jki} and λ_{ki} are integrals which represent the overlap between the gain and mode profiles where

$$\gamma_{ki} = \frac{2}{W^2} \int_0^W J_0(\sigma_i r/W) \psi_k(r) r dr$$

$$\phi_{jki} = \left(2 / (W^2 J_0^2(\sigma_j)) \right) \int_0^W J_0(\sigma_i r/W) J_0(\sigma_j r/W) \psi_k(r) r dr$$

$$\lambda_{ki} = (2/W^2) \cdot \int_0^W J_0(\sigma_i r/R) \psi_k(r) r dr$$

D. Optical output power modeling

The photon number S_k in each mode can be related to the corresponding optical output power P_k using

$$P_k = k_{fk} S_k,$$

where k_{fk} is the output-power coupling coefficient of mode k .

Complete model

The VCSEL can be described as a four-port device, pe , ne are the input ports, and po , no are the output ports, respectively. The symbol is illustrated in Fig.2 (a). The equivalent circuit of VCSEL is composed of input sub-circuit, temperature sub-circuit, zero order sub-circuit, j th order sub-circuit, k mode optical sub-circuit, and output sub-circuit, as shown in Fig.2 (b).

In input sub-circuit, pe and ne are the VCSEL's electrical interface. C_p is the pad capacitance, L_p is a series inductance representing the wirebond, and R_p is the contact resistance, respectively. C_s is the parasitic capacitance of Bragg mirrors, R_s is the parasitic resistance of Bragg mirrors, respectively. The input voltage-current characteristic is modeled by a laser diode including the effect of the temperature dependent parasitic resistance and reverse saturation current instead of a controlled voltage source.

In the temperature sub-circuit, td is the terminal which models the temperature T . The sub-circuit elements are given as

$$C_{th} = \tau_{th}/R_{th};$$

$$I_{tem} = T_0/R_{th} + I_{tot}V - \sum_k P_k$$



(a)

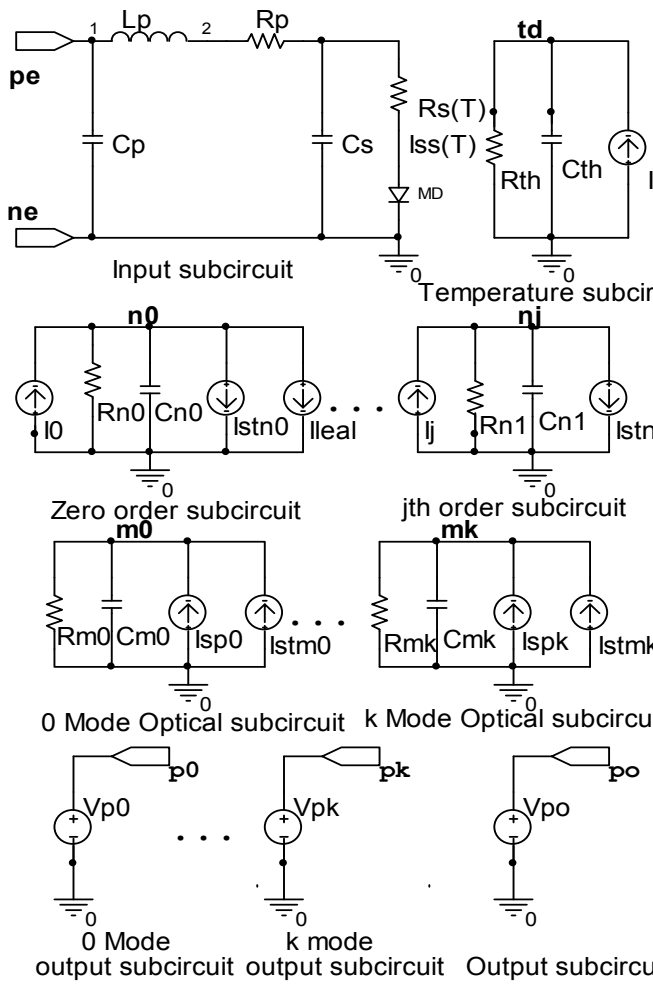


Fig.2 VCSEL model (a) symbol (b) equivalent circuit

In zero order sub-circuit, n0 is the terminal whose node voltage models the zero order carrier number. The sub-circuit elements are given as

$$I_0 = \eta_i I / (v_{n0} + \delta_n); \quad R_{n0} = \tau_n / qz_n; \quad C_{n0} = 2qz_n$$

$$I_{stdn0} = qz_n \delta_n / \tau_n + qG_0 (a_0 + a_1 v_{id} + a_2 v_{id}^2)$$

$$\sum_k \left[\frac{\gamma_{k0} z_n (v_{n0} + \delta_n)^2 - \sum_{i=1}^{\infty} \gamma_{ki} z_n v_{ni} - \gamma_{k0} N_{T0} (c_0 + c_1 v_{id} + c_2 v_{id}^2)}{(v_{n0} + \delta_n)(b_0 + b_1 v_{id} + b_2 v_{id}^2)} S_k \right]$$

$$I_{leak} = \frac{I_{I0}}{(v_{n0} + \delta_n)} \exp \left[\left(\frac{-d_0 + d_1 z_n (v_{n0} + \delta_n)^2 + d_2 v_{id} z_n}{(v_{n0} + \delta_n)^2 - d_3 / z_n (v_{n0} + \delta_n)^2} \right) / v_{id} \right]$$

In jth order sub-circuit, nj is the terminal whose node voltage models the jth order carrier number. The sub-circuit elements are given as

$$I_j = \eta_j \varepsilon_j I; \quad R_{nj} = -\tau_n / (qz_n (1 + h_j)); \quad C_{nj} = -qz_n$$

$$I_{stdnj} = qG_0 ((a_0 + a_1 v_{id} + a_2 v_{id}^2) / (b_0 + b_1 v_{id} + b_2 v_{id}^2))$$

$$\sum_k \left[\frac{\phi_{jk0} z_n (v_{n0} + \delta_n)^2 - \sum_{i=1}^{\infty} \phi_{jki} z_n v_{ni} - \phi_{jk0} N_T(T)}{1 + \sum_m \varepsilon_{mk} S_m} S_k \right]$$

In the optical sub-circuit, mk is the terminal whose node voltage models the phonon number in the kth mode. The sub-circuit elements are given as

$$R_{mk} = k_{fk} \tau_{pk}; \quad C_{mk} = 2/k_{fk}$$

$$I_{spk} = (\beta_k / \tau_n (v_{mk} + \delta_m)) \left[l_0 z_n (v_{n0} + \delta_n)^2 - \sum_{i=1}^{\infty} l_i z_n v_{ni} \right]$$

$$I_{item}^{smk} = \frac{G_T}{(v_{mk} + \delta_m)} \frac{\left[\lambda_{k0} z_n (v_{n0} + \delta_n)^2 - \sum_{i=1}^{\infty} \lambda_{ki} z_n v_{ni} - \lambda_{k0} N_T \right] S_k}{1 + \sum_m \varepsilon_{mk} S_m} \frac{\delta_m}{k_{fk} \tau_{pk}}$$

In the kth mode output sub-circuit, pk is the terminal whose node voltage models the kth mode optical output power P_k .

In the output sub-circuit, po is the terminal whose node voltage models the total optical output power P_o

$$P_o = \sum_k P_k$$

In the expressions of circuit elements above, δ_n , δ_m , and z_n are arbitrary constants to improve convergence.

Example simulation and discussion

In order to demonstrate the ability of our VCSEL model to replicate the basic thermal, spatial and multimode behavior of actual VCSEL operation, we implemented our model into a conventional SPICE-like simulator. We generated example simulations of the two-mode VCSEL under dc, ac, and transient conditions. The parameters are taken from references [10]. In the simulations, mode 0 represent LP01, and mode 1 represent LP11. The results allowed us to verify that our model is capable of replicating the basic thermal and spatial behavior typical of VCSEL.

Fig. 3 illustrates the variation of N_0 , N_1 and N_2 for the 25°C and 40°C LI curve. As the current increases, N_1 and N_2 begin to increase because of spatial hole burning. N_0 also begins to increase in order to maintain an above-threshold modal gain.

Fig.4 illustrates the VI characteristics and LI characteristics for the two-mode VCSEL with leakage at various ambient temperatures of 25°C and 40°C. As LI curves shown, the threshold current of VCSEL is depended by temperature and output power rollover. The mode 1 has a higher threshold. Once the mode 1 begins to lase, there is a kink in the output power of mode 0. As VI curves shown, while the inject current increased, the parasitic resistor will decrease, and saturation current will increase.

Fig. 5 illustrates the resulting transfer function at ambient temperatures of 25 and 40°C. The resonance frequency decreases with temperature. The amplitudes of mode 1 are much smaller than mode 0.

Fig. 6 illustrates the transient response to a square-pulse-train input current at various ambient temperatures of 25°C and 40°C. Similar to Fig.4, there is an additional delay before the mode 1 can lase because of SHB. This result provided an initial verification of our model's spatial capabilities. This result provided an initial verification of our model's thermal, spatial and multimode capabilities.

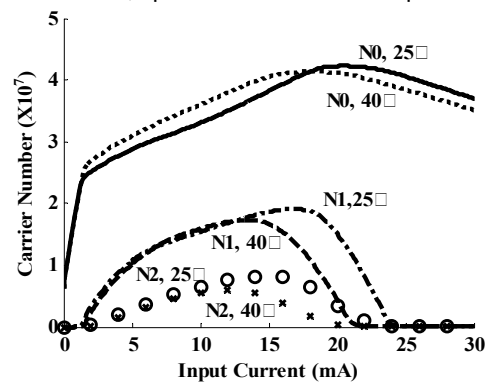


Fig.3 Variation of N_0 , N_1 and N_2

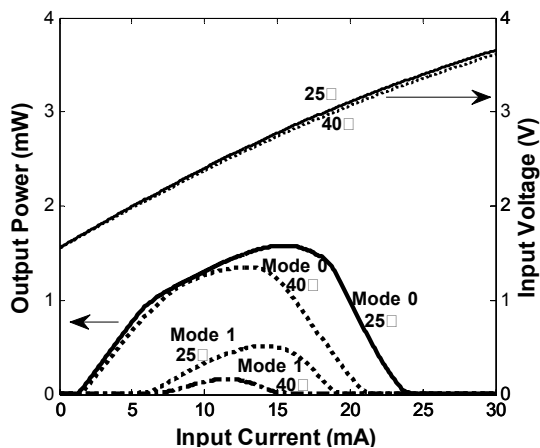


Fig.4 Simulated VI curves and LI curves of the two-mode VCSEL with leakage

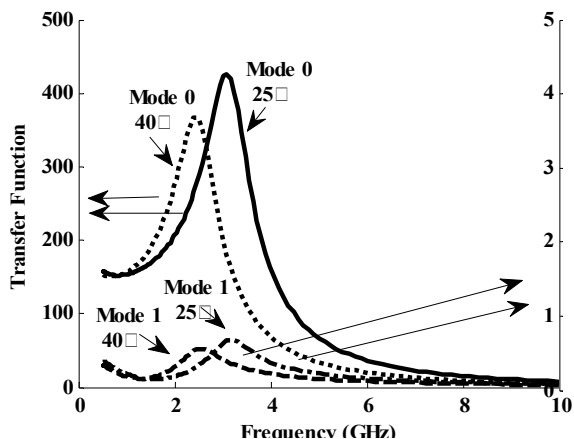


Fig.5 Simulated transfer function of the two-mode VCSEL

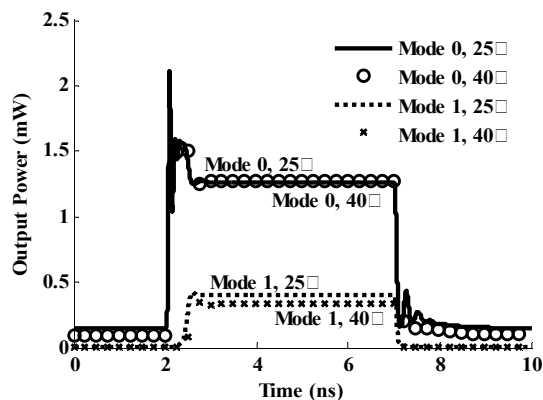


Fig.6 Simulated transient response of the two-mode VCSEL

Conclusions

In this paper, we present a comprehensive circuit-level VCSEL model that addresses the spatial and thermal behavior of VCSEL based on the multimode rate-equations. A general diode, including the thermal effect of parasitic resistor and reverse saturation current, instead of an empirical function, is adopted to model the current-voltage relationship. The model is more comprehensive and parameters are easier to determine. The equivalent circuit of the model and expressions of circuit elements are given. It is really simple, and it can model basic laser behavior under both dc and non-dc conditions. The simulated dc, ac and transient features compare favorably with references.

ACKNOWLEDGMENTS

This work was supported in part by NSFC under Grant No. 51107089, Grant No. 60976067 and Grant No. 61106067 as well as partially supported by the Youth Chenguang project of Science and Technology of Wuhan City of China under Grant No 201050231056.

REFERENCES

- [1] Massart Thierry, Meuter Cedric, V B Laurent, Inform. Process. Lett. 106 (2008) 120-126
- [2] Koyama, F., Miyamoto, T., IEEE 19th International Conference on Indium Phosphide & Related Materials, (2007) 420 – 425.
- [3] Gatto, A., Boletti, A., Boffi, P., et. all. IEEE Photonics Technology Letters, Vol.21, No.12, (2009) 778-780.
- [4] Chao-Kun Lin, Tandon, A., Djordjev, K., et. all. IEEE J. Selected Topics in Quantum Electronics, 13 (2007) 1332-1339.
- [5] W. M. Man and S.-F. Yu. IEEE J. Select. Topics Quantum Electron., 4 (1998) 715-722.
- [6] Mena, P. V., Morikuni, J. J., Kang, S. M., et. all. IEEE J. Lightwave Technol., 17 (1999) 865-872.
- [7] Liu Jie, Chen Wen-lu, and Li Yu-quan. J. Zhejiang Univ. Science A, 7 (2006) 1968-1972.
- [8] Liang Feng, Gao Jianjun, and Tian Xuenong. Chinese J.Semiconductors, 28 (2007) 1125-1129.
- [9] J. J. Morikuni, P.V. Mena, A. V. Harton, et al. IEEE J. Lightwave Technol., 17 (1999) 95-102.
- [10] Mena, P. V., Morikuni, J. J., Kang, S. M., et. all. IEEE J. Lightwave Technol., 17 (1999) 2612-2632.
- [11] Gao Jianjun, Li Xiuping, and Flucke J. IEEE J. Lightwave Technol., 22 (2004) 1604-1611.

Authors: prof. dr Xinzhi Shi, Institute of Microelectronics & Information Technology, Wuhan University, Wuhan 430079, China, E-mail: shi_xinzhi@163.com